Use of positron emission particle tracking to assess mixing of a graphite-based lithium-ion anode slurry in an Eirich mixer

Hare, S.D.; Werner, D.; Windows-Yule, C.R.K.; Wheldon, T.Z. Kokalova; Kendrick, E.; Simmons, M.J.H.

DOI:
10.1016/j.cherd.2023.08.007

Document Version
Publisher's PDF, also known as Version of record

Citation for published version (Harvard):
Hare, SD, Werner, D, Windows-Yule, CRK, Wheldon, TZK, Kendrick, E & Simmons, MJH 2023, 'Use of positron emission particle tracking to assess mixing of a graphite-based lithium-ion anode slurry in an Eirich mixer', *Chemical Engineering Research and Design*, vol. 197, pp. 509-518. https://doi.org/10.1016/j.cherd.2023.08.007

Available online at www.sciencedirect.com

Chemical Engineering Research and Design

journal homepage: www.elsevier.com/locate/cherd

Use of positron emission particle tracking to assess mixing of a graphite-based lithium-ion anode slurry in an Eirich mixer

S.D. Hare[a,*], D. Werner[a], C.R.K. Windows-Yule[a], T.Z. Kokalova Wheldon[b], E. Kendrick[c], M.J.H. Simmons[a]

[a] School of Chemical Engineering, University of Birmingham, Edgbaston, Birmingham, B15 2TT, UK
[b] School of Physics and Astronomy, University of Birmingham, Edgbaston, Birmingham, B15 2TT, UK
[c] School of Metallurgy and Materials, University of Birmingham, Edgbaston, Birmingham, B15 2TT, UK

ARTICLE INFO

Article history:
Received 2 May 2023
Received in revised form 3 August 2023
Accepted 4 August 2023
Available online 9 August 2023

ABSTRACT

The mixing of electrode slurries is a key processing step during the manufacturing of lithium-ion batteries, and poor mixing can have a profound effect on final cell electrochemical performance. This is complicated by the evolving non-Newtonian rheology of these slurries. In this study, Positron Emission Particle Tracking (PEPT) is used to determine the fluid dynamics and dispersion of a model graphite-based anode slurry in an Eirich EL1 mixer, equipped with a rotating pan, wall scraper and internal rotor. The main processes studied are the wetting of graphite particles and breakup of large graphite agglomerates. For experiments performed at different internal rotor tip speeds, with fixed outer pan speed, the dispersion dynamics change with the lowest rotor speed (2 m/s) leaving a large channel of poor mixing between the rotor region and the rotating pan, whilst the mixing within the vessel is mainly driven by the rotating pan. At higher mixing speeds (6 and 10 m/s) more of the vessel volume is active and there is no longer a poor mixing region observed, with 10 m/s tip speed producing the highest intensity of dispersion. An increasing mixer effectiveness (average dispersion across the mixing vessel) as well as an increasing dispersion co-efficient (rate of mixing) is also observed, which will be use to inform scale-up criteria.

1. Introduction

Lithium-ion battery manufacturing is a complex, multistage process, carried out across a wide variety of length and time scales (Kwade et al., 2018). Traditionally, the impact of each processing step is often only considered in terms of its sufficiency for the subsequent step, with the final performance of the cell only given scrutiny once manufactured (Bockholt et al., 2016). Thus, issues with upstream processing are difficult to diagnose and require significant amounts of time for troubleshooting. There is significant scope and industry interest to develop physical and chemical models from better understanding of each processing step (Grant et al., 2022). In particular the formulation and mixing of the electrode materials to form a slurry in the early part of the process is critical, before they are coated onto a metal substrate to form a battery component (Reynolds et al., 2021).

The mixing of anode slurries is complicated by the initial wetting of the hydrophobic graphite powder, typically 95 wt % of the solids within the slurry (Lee et al., 2005). This tends to be more of an issue with non-contact planetary mixers whereas the dual-asymmetric mixer has a wall-scraper to assist in the breakup of the dry powder. The next step involves homogeneous dispersion of carbon black conductive

* Corresponding author.
E-mail address: s.d.hare@bham.ac.uk (S.D. Hare).

https://doi.org/10.1016/j.cherd.2023.08.007

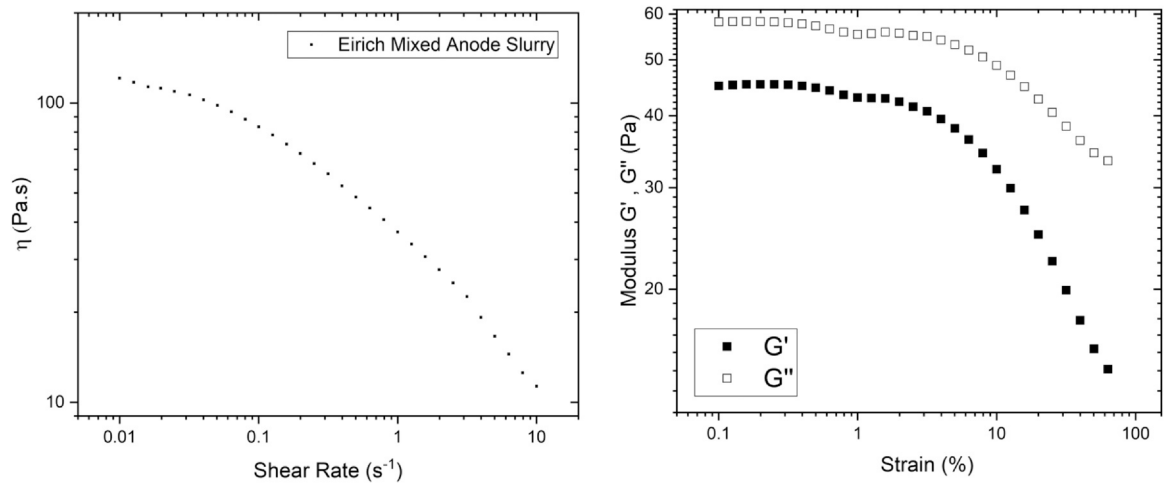

Fig. 1 – Flow curve and amplitude sweep of anode slurry mixed with the Eirich mixer at 10 m/s for 20 min.

additive throughout the slurry, which requires good levels of both dispersive and distributive mixing (Paul and Atiemo-Obeng, 2004) as the nanoparticulate carbon agglomerates easily. One way of overcoming this issue is to ensure a sufficient mixing time (Grießl et al., 2021), as well as minimising any dry powder premixing (Bauer et al., 2015). Otherwise, the carbon black coats the graphite, leaving less free to form conductive chains throughout the slurry once coated onto the electrode substrate (Wang et al., 2020).

The rheology is a critical property for the final slurry as it affects its coatability onto the electrode substrate. The slurry needs to possess the correct consistency to be able to flow through the coater and then maintain its shape once coated. The rheology is a strong function of the slurry microstructure, (Reynolds et al., 2022; Sung et al., 2020; Hawley, 2019) which is governed by both the formulation and the mixing protocol. Poorly mixed inks tend to have a higher consistency and grainy appearance due to agglomerates not being fully broken down, and particles being poorly covered with polymer binder.

Characterisation of the slurry mixing is therefore a key step. The complex non-Newtonian rheology of battery slurries prohibits the establishment of transparent mimic fluids suitable for measurements of mixing using optical methods. This coupled with the complex, opaque mixer designs (see Fig. 3) introduces another layer of challenge in directly measuring mixing of industrially relevant formulations in industrially relevant mixers.

However, Positron Emission Particle Tracking (PEPT) provides the ability to track a radioactive particle in opaque systems and mixers using the actual slurries (Barigou, 2004), and correlates accurately with other optical tracking techniques such as Particle Image Velocimetry (PIV) (Pianko-Oprych et al., 2009). PEPT is a non-invasive tracking technique used to track complex flows in opaque systems and equipment, with some applications including coffee roasters (Al-Shemmeri et al., 2021), fluidised beds (Windows-Yule et al., 2020b), static mixers (Marjan Rafiee et al., 2013), and stirred tanks (Katie Cole, 2022; Guida et al., 2010).

In this work, PEPT is used to determine the fluid dynamics and dispersion for a model graphite-based anode slurry in a nominal 1 L capacity Eirich EL1 mixer, as CMC and graphite predominantly dictate the rheology of anode slurries (Reynolds et al., 2022). Understanding the flow behaviour in a mixing vessel is key to predicting the success (or lack thereof) of the key processing steps of both wetting the graphite with CMC, and also breaking down the graphite agglomerates. Mixing speeds of 2, 6 and 10 m/s rotor tip speed were selected due to their use in mixing different components in battery electrode slurries. 2 m/s is a low speed for the Eirich mixer, making it suitable for the incorporation of a common secondary binder, styrene butadiene rubber (SBR), as it can be deformed or broken-up by high shear. SBR is added to water based anodes in conjunction with carboxymethyl cellulose (CMC) (Buqa et al., 2006) to enhance coating flexibility which minimises cracking/flaking of the electrode coating from the current collector. 10 m/s is a speed more suitable for the wetting of graphite with CMC/water, and 6 m/s was chosen as intermediate speed.

2. Materials and methods

2.1. Slurry composition

A 1.5 wt% CMC (Ashland BVH8) solution in water was predispersed using a Turbula T 2 F mixer for 16 h. This solution was then mixed together with graphite (Targray BFC-QC) in the Eirich mixer to produce slurries of 50 % w/w graphite, with a fully mixed slurry having a Reynolds number of between 0.8 and 3.8 depending on the Eirich's rotor tip speed.

The final slurry rheology is highly dependent on the microstructure within the slurry, with properly mixed slurries being shear-thinning visco-elastic fluids with a low-shear plateau, and poorly-mixed slurries being shear-thinning weak colloidal gels that do not always have an apparent low-shear plateau. An in-depth study of the rheology and microstructure of slurries using the same composition can be found here (Reynolds et al., 2022).

Fig. 1 shows the shear-thinning behaviour of a well mixed anode slurry, with the viscosity at low shear-rates being around 130 Pa s and at 10 s^{-1} being around 10 Pa s. The visco-elastic behaviour is predominantly fluid-like due to the viscous modulus G″ being greater than the elastic modulus G′ at all strains.

2.2. Mixer geometry

An Eirich EL1 mixer (nominal capacity 0.3–1 L) equipped with a pin-type rotor was used, at rotor tip speeds of 2, 6 and 10 m/s (500–2400 rpm), which were set to co-rotate with the mixing

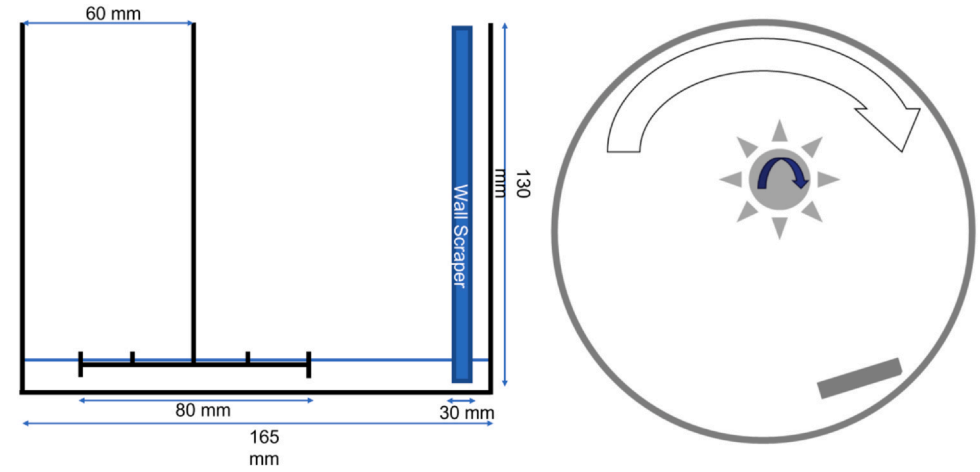

Fig. 2 – Side on to-scale schematic of Eirich EL1 mixer, and top down estimated schematic of the Eirich mixer, showing offset nature of the rotor. Gap between scraper and wall 3.5 mm, impeller clearance from base 15 mm. Blue horizontal line indicates approximate slurry height.

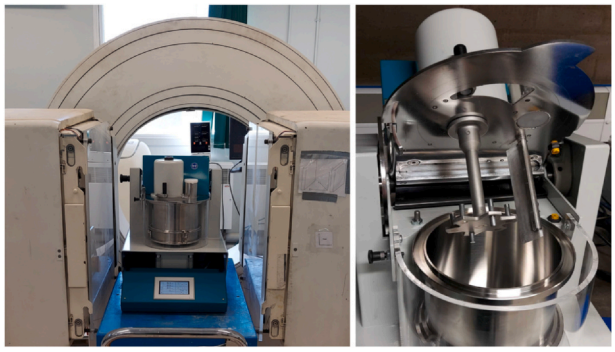

Fig. 3 – Eirich mixer in the ADAC Forte camera and a picture of the open Eirich mixer.

pan rotation set constant at 0.5 m/s (58 rpm), a diagram and picture of the mixer are shown in Figs. 2 and 3 respectively, with Fig. 3 showing the rotor raised out of the mixing pan. The pin-type rotor consists of a flat plate in the shape of a 6 pointed star with rounded tips, with 6 upwards facing pins and 2 shorter downwards facing pins. The downwards facing pins being on opposite sides of the rotor. The vessel was filled with 350 g of fluid to a height of 15 mm, to which 350 g of graphite was added, resulting in approximately 0.5 L of slurry. The approximate slurry height is indicated with the blue line in Fig. 2. Whilst this is not full capacity of the mixer, it is within the nominal volume for operation given by the manufacturer. Furthermore, in feasibility and scale-up experiments, not running at full volume is advantageous to minimise material wastage. The fill height is low when compared to a stirred tank due to the dimensions of the mixing pan needing to accommodate the option to angle the pan (more commonly done when used for granulation). Due to the complexity of the enclosed mixer design, it was not possible to measure the power input into the fluid using a torque meter.

The pan rotation speed was kept constant which allowed only the impact of the rotor speed to be studied, as well as keep a constant Froude number of 0.39 for the system. This is due to the low fill height of the vessel, and the centrifugal force within the vessel arising from the pan rotation, making the pan diameter the characteristic length-scale.

2.3. PEPT measurements

For the PEPT measurements, the Eirich mixer was placed between the two detectors of a modified ADAC Forte camera, so that the mixing pan was in the centre of the detectors, with the detectors then moved as close as possible to give maximum data rate and minimise scatter. More information on the ADAC camera can be found here (Parker et al., 2002). A neutrally buoyant ion-exchange resin bead of approximately 300 μm was used to measure the flow during mixing. The resin was labelled with the β^+-emitting radioisotope Fluorine-18, through immersion in a solution containing free ^{18}F ions. Full details of this process, known as *indirect activation*, can be found in references (Windows-Yule et al., 2022; Parker, 2008).

The tracer was located using the PEPT-ML algorithm (Nicuşan and Windows-Yule, 2020), where the tracer location is computed from the gamma ray line of responses (LoRs) and then clustered to improve precision, trajectories were then calculated, as well as tracer velocity. PEPT-ML was determined to be the best choice for the present experiment as from a recent benchmarking study (Windows-Yule, 2022) it has been shown to possess the best combined spatial and temporal resolution of currently-available algorithms, making it well suited for the system of interest.

The dispersive mixing rate was calculated as described by (Windows-Yule et al., 2020a; Werner et al., 2023), in which tracer locations with a similar "start point" are grouped together and their spread measured after a given time-step. An example of low and high dispersion is shown in Fig. 4. The mixer effectiveness (ME) as described by Martin et al. is then quantified by averaging all the dispersion values across the mixer for that time-step (Martin, 2007).

$$ME = \frac{1}{N_p} \sum_{k=1}^{N_c} \sigma_k^2 n_{p,k} \tag{1}$$

where N_p is the number of passes through all N_c cells, σ_k is the cell dispersion value, and n_p the number of passes in each cell k.

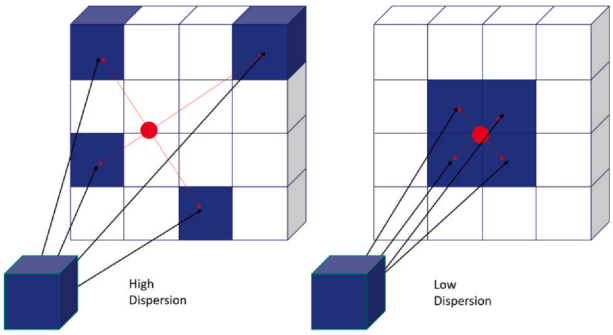

Fig. 4 – Diagrams of high and low dispersion.

3. Results and discussion

3.1. *Tracer occupancy and velocity*

Tracer trajectories are used to build up an occupancy profile across the vessel, by subdividing the vessel into regions of interest, and then counting the tracer trajectories within that region of interest. This then builds a Eulerian grid of the vessel showing which location of the vessel the tracer has occupied, and to what degree. A deeper explanation can be found here (Windows-Yule, 2020).

For all mixing speeds, the tracer occupies the vast majority of the vessel occupied by the fluid, albeit with a lower occupancy in the immediate vicinity of the rotor head (as seen in Fig. 5a). There is a region of increased occupancy around the wall scraper as the flow is disrupted, with an inner ring present at 2 m/s tip speed, again seen in Fig. 5a.

The low occupancy region around the rotor head (Fig. 5a) corresponds to the highest region of tracer velocity, as shown in Fig. 5b. Fig. 5b also shows that the narrow region between the rotor head and the wall (top right of image) is the second highest region for velocity, as is to be expected due to the shorter distance between the rotor and spinning pan wall. After the flow is disrupted by the wall scraper, the tracer velocity drops significantly, before gradually picking up speed again as it circulates around the mixing vessel. There is also no difference in tracer velocity between the inner occupied area and the outer ring in which the tracer sometimes becomes trapped. Having a tracer be able to move freely throughout the whole vessel is important for operation, as it shows no dead-zones within the mixer.

3.2. *Mixer effectiveness*

Considering a mixer holistically is important when choosing mixer type and parameters for a manufacturing process; mixer effectiveness (ME) gives an insight into the overall dispersion and hence level of mixing achieved by a mixer for a given material, and as such is an excellent starting point. Values of ME were calculated as the average dispersion across the vessel for each dispersion time-step from approximately 45 min of data at each value of rotor tip speed. 45 min of data was used to build up a sufficient body of tracer locations to ensure ergodicity of the tracer particle and to minimise the impact of any short periods when the tracer became stuck to a surface in the mixer. Fig. 6 shows the mixer effectiveness (ME) for 3 different tip speeds; the plateau value for ME depends on the volume occupied by the tracer during mixing and is limited by the physical dimensions of the vessel. The variation in values between rotor speeds is due to the material being centrifuged further up the sides of the vessel as the rotor speed increases, as well as the void around the rotor head increasing with rotor speed. At very short time-steps all rotor speeds have a similar ME but between 1 s and 2 s, the 10 m/s speed has the highest ME value. Both 2 m/s and 6 /s speeds have a similar ME value initially. It is clear in Fig. 6 that as rotor tip speed increases more dispersion and mixing is happening.

Whilst more mixing is a key finding, it is also important to assess how quickly the mixing is occurring within the vessel, this is possible by calculating the gradient of the initial linear regime of ME, the dispersion co-efficient.The linear region is where dispersion (and thus ME) is not affected by vessel size/walls and was estimated to be the first 12 points, which were used to calculate the dispersion co-efficients in Table 1. Dispersion co-efficient increases with rotor speed, meaning that not only is more mixing occurring, but it is also happening faster.

3.3. *Active mixing volume*

Whilst the overall value of ME is a useful metric, it is a complex function of the fluid dynamics/mixing intensity and the active mixing volume. The degree of dispersion and fluid dynamics were thus assessed locally to help devise criteria for optimal operation.

Fig. 7 shows heat-maps of dispersion values for the 2 m/s rotor speed at 1 s and 5 s time-steps. At the 1 s time-step (7a), there are two discrete regions of activity within the mixer. The first, around the rotor head, is relatively uniform, but with a region of slightly higher dispersion in the narrower section where the rotor is closer to the pan wall, due to a higher tracer velocity in this region (thus allowing it to travel further in a fixed time-step). The second region of mixing is at the pan wall, with a particular “hot-spot” around the fixed wall scraper, this is due to the significant disruption of fluid flow caused by the scraper. Whilst the 5 s heat-map (7b) is past the linear regime used to define the dispersion co-efficient, and is when the movement of the tracer has begun to be affected by vessel wall, it is still useful in visualising the how the tracer can become trapped in the outer ring of the vessel, and when the tracer eventually manages to escape this region and move into the centre of the vessel (resulting in the inner ring of high dispersion).

As the dispersion time-step is lengthened it is possible to observe these two regions grow and eventually meet one another, shown by the inner ring of apparent high dispersion in Fig. 7b. For some periods during mixing, the tracer can become trapped within the outer ring zone for a short period of time, which is much more prevalent at lower mixing speeds. The outer region in which the tracer can become trapped varies in size depending on rotor speed. It is largest at 2 m/s tip speed as seen in Fig. 7b (and is also reflected in the tracer occupancy shown in Fig. 5a), as the rotor speed increases it decreases in size. This is due to the competing phenomena of the fluid being pushed out by the rotor and fluid being pushed inwards by the rotating pan wall.

The dispersion within the vessel is a function of both the central rotor and the rotating pan (and wall scraper), possibly leading to areas of lower dispersion within the mixer that are not necessarily captured by the overall value of ME. However, the distribution of dispersion values for each dispersion time-step and mixer speed can be plotted to show how the different regions of the mixer behave, which when combined

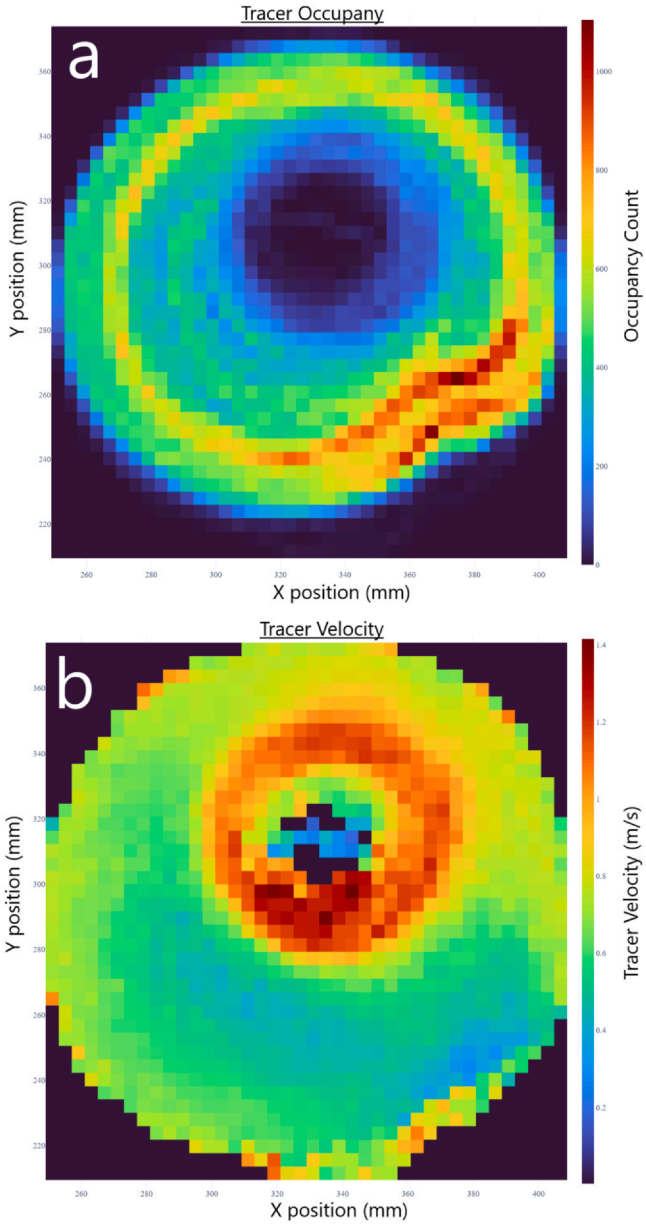

Fig. 5 – Top down depth-averaged tracer occupancy (a) and depth-averaged tracer velocity (b) for the initial 15 mins of mixing at 2 m/s tip speed. Wall-scraper is at the bottom right of each image.

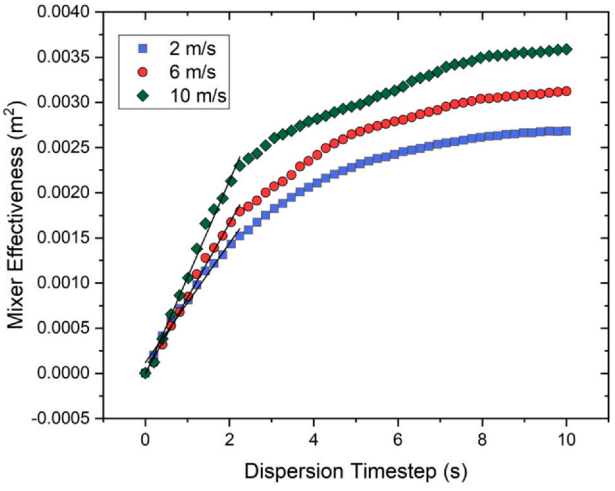

Fig. 6 – Mixer effectiveness values with a fit of dispersion co-efficient for the Eirich mixer at different rotor speeds.

Table 1 – Dispersion co-efficient values for the Eirich mixer at 2, 6 and 10 m/s tip speed.

Mixer Tip Speed (m/s)	Dispersion Co-efficient (m^2/s)
2	6.61×10^{-04}
6	8.30×10^{-04}
10	1.00×10^{-03}

give the ME value. Fig. 8 shows how the distribution of dispersion values for a 2 s time-step vary between a rotor speed of 2, 6 and 10 m/s, the number of zones in the dispersion calculation are kept the same for each mixing speed.

For the 2 m/s rotor speed, there is a significantly more very low dispersion regions in the vessel when compared to the 6 and 10 m/s data. As seen in Fig. 7a, for a 2 s dispersion time-step, the majority of mixing is occurring at the pan edge. This could explain the large peak in Fig. 8 for the 2 m/s data at around 0.0018 m^2 dispersion. 6 and 10 m/s have broadly the same shape, with both having less very low

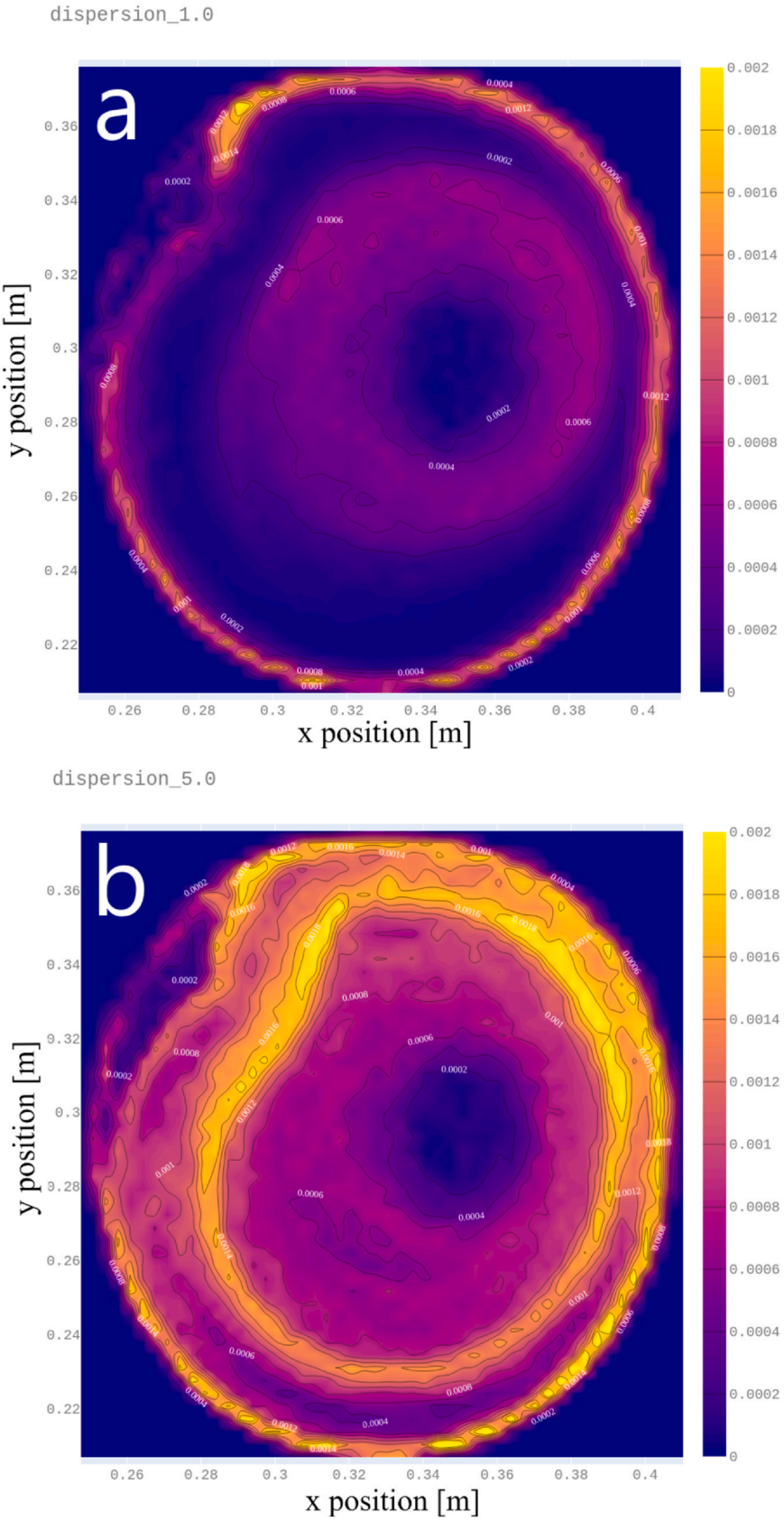

Fig. 7 – Depth-averaged heatmaps of dispersion values for different dispersion time-steps, 1 s (a) and 5 s (b) for the Eirich mixer at 2 m/s rotor tip speed. Dead zone in both images is the location of the rotor head. Wall-scraper is at the top left of each image.

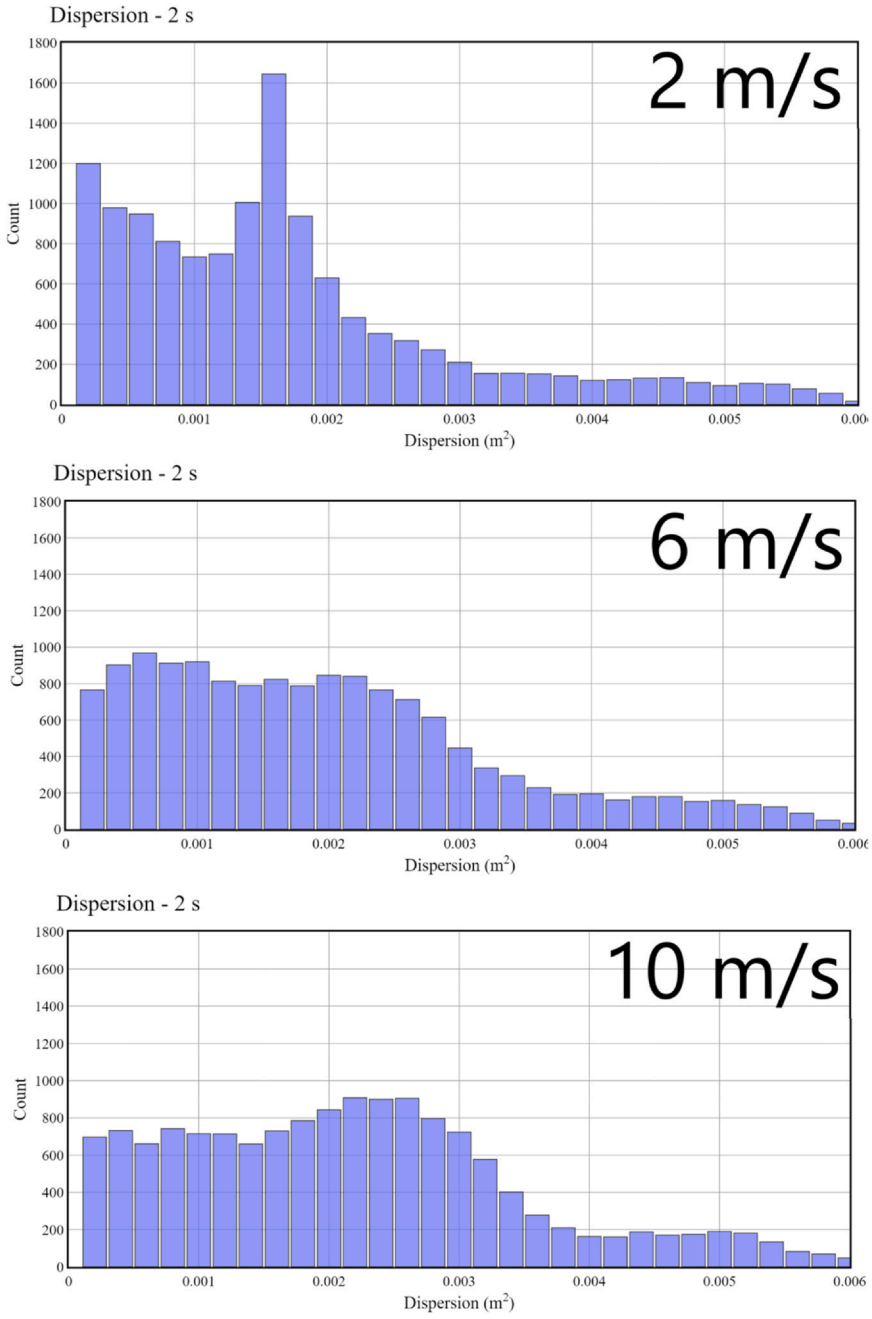

Fig. 8 – Histograms of dispersion data at a 2 s time-step for 2, 6, and 10 m/s tip speed.

dispersion regions than 2 m/s, and neither having a sharp peak in dispersion. They both show a good general level of mixing activity, with 10 m/s being slightly shifted to higher dispersion values.

3.4. *Low speed mixing*

Showing the dispersion within the vessel in three dimensions makes this difference between the 2 m/s mixing and the high speed mixing more apparent. Fig. 9a shows that the edge of the moving mixing pan is where most dispersion is occurring at 2 m/s tip speed, and that there is far lower mixing occurring around the rotor. This shows that at this mixing speed, the mixing in the vessel is mainly due to the rotating mixing pan, and not due to the rotor head. There is also a channel region between these two mixing areas where there is no apparent dispersion occurring, this is most likely due to the low power input from the rotor being dissipated by the extremely viscous slurry during mixing (Reynolds et al., 2022). This is also exacerbated by the fact that un-wetted graphite is hydrophobic, so forms large agglomerates and localised network structures, meaning it is highly likely that the viscosity of a partially mixed slurry will be higher than one that has been fully mixed, making 2 m/s an unsuitable speed for the mixing of the graphite in CMC.

However, as stated in the introduction, SBR must be mixed at low speed, but still needs to be distributed homogeneously throughout the slurry to enhance coating flexibility and adhesion to the current collector. Whilst the ME and dispersion co-efficient are lower for 2 m/s it may be possible to ensure homogeneous mixing of the SBR by ensuring a longer mixing time. However, this may be complicated by the limited amount of overall mixing at 2 m/s, as well as the extremely localised mixing at the pan edge and wall scraper. This is performed as a separate mixing step to

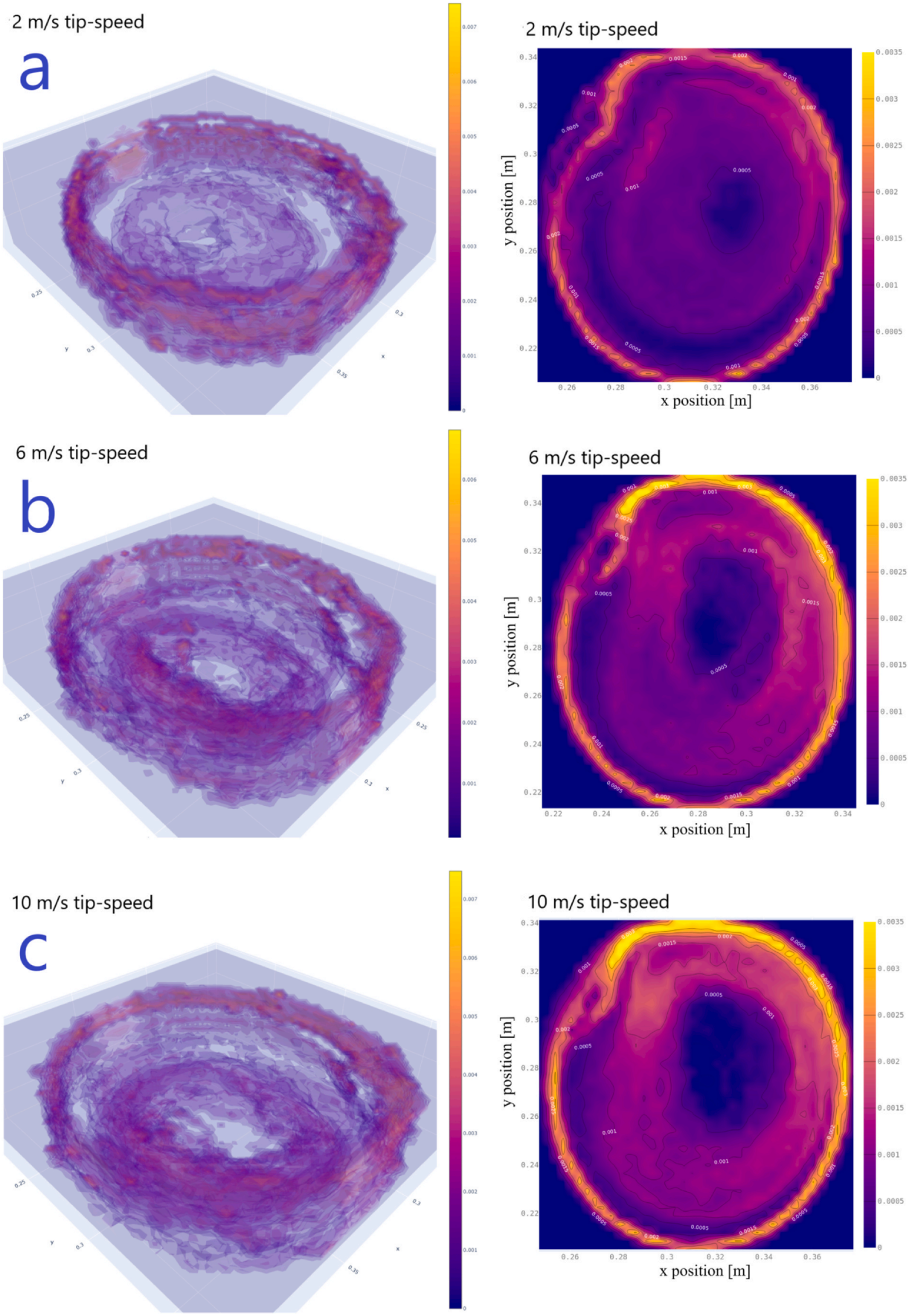

Fig. 9 – 3D and 2D depth-averaged plots of dispersion values (2 s time-step) for tip speeds of 2 (a), 6 (b) and 10 m/s (c). Wall-scraper is at the top left of each 2D image.

the graphite wetting so does avoid the issues with partially mixed slurries mentioned above.

One way of assessing this in the future would be using Positron Emission Projection Imaging (PEPI), where a small volume of radioactive tracer fluid and measuring the concentration gradient as the fluid is incorporated into the slurry (Simmons et al., 2009), and would give an excellent indication of the incorporation dynamics of adding SBR. Whilst this experiment would give good insight into the distribution of SBR throughout the slurry, it would be of little value in determining the overall system dynamics, as done in this work. This is because it would only provide a short snapshot of data until the initially localised area of high response would dissipate to a homogeneous background level as the fluid was distributed throughout the slurry.

3.5. *Intermediate and high speed mixing*

At 6 m/s tip speed, there is a sharp reduction in the number of lowest value areas of dispersion in Fig. 8 and no peak dispersion value similar to that seen at 2 m/s. There is a general shift to higher dispersion values, suggesting more of the vessel is active in terms of mixing. This is seen clearly in Fig. 9b where there is no channel of little to no mixing occurring in the 6 m/s 3D plot. It shows much more mixing occurring in the central area of the mixer, suggesting the power input from the rotor is sufficient to generate mixing from both the rotor tip and as well as that from the rotating pan.

For 10 m/s (Fig. 9c) the same general shape as 6 m/s is seen, but with again another shift to higher dispersion values. Figs. 8 and 9c show how the vast majority of the vessel behaves similarly to the speed of 6 m/s, but now there is a greater intensity of mixing happening in the central area. This suggests that both 6 and 10 m/s are suitable for the mixing of graphite in CMC for anode slurries, and that efficiencies may be found in process optimisation to achieve sufficient mixing for the minimum power input.

4. Conclusions

PEPT has been used to characterise the mixing and dispersion rate of a model Li-ion anode slurry in an Eirich EL1 mixer. Two main regions of mixing were identified, one surrounding the internal rotor head and one at the wall edge and scraper. Mixer effectiveness was calculated for three different mixing speeds, and the dispersion co-efficient was then calculated from the ME values. Both ME and dispersion co-efficient are found to increase with rotor tip speed.

At 2 m/s tip speed, the mixing within the vessel is predominantly driven by the rotating pan, resulting in large regions of the vessel having little to no dispersion occurring within them, this is observed both in histograms of dispersion values as well as 3D plots of the vessel. At 6 and 10 m/s more of the vessel is active and mixing is driven by both the rotor movement as well as the rotating pan, resulting in a greater degree of mixing at both of these speeds, with 10 m/s being more intense.

When considering the aims of breaking down graphite agglomerates and sufficiently wetting the graphite to incorporate it into the slurry, 2 m/s does not appear suitable, due to the regions of little to no dispersion. These regions are likely to become larger as the mixer size is scaled up, so are a key feature of the flow behaviour to be considered for scale-up criteria. As these regions appear to be due to the difference in tip-speed and pan rotation speed, it is of interest to better understand how they interact at different pan speeds and scales.

Whilst low tip speeds clearly lead to sub-optimal mixing throughout the vessel, SBR, a secondary polymer binder in water-based anode slurries cannot be mixed at high shear, so extended mixing is most likely required to fully disperse this throughout a mixed slurry. Both 6 and 10 m/s appear suitable for the mixing of graphite and CMC for anode slurries, with there being clear mileage in process optimisation to find the best balance in terms of power input and mixing outcome, which becomes ever more important at the large-scale end of the Eirich mixer design.

Declaration of Competing Interests

The authors declare that they have no known competing financial interests or personal relationships that could have appeared to influence the work reported in this paper.

Acknowledgements

Special thanks to Leonard Nicuşan for his assistance with the PEPT library code-base. This work was supported by the Faraday Institution NEXTRODE project (faraday.ac.UK; EP/S003053/1, FIRG015).

References

Al-Shemmeri, Mark, Windows-Yule, Kit, Lopez-Quiroga, Estefania, Fryer, Peter J., 2021. Coffee bean particle motion in a spouted bed measured using Positron Emission Particle Tracking (PEPT). J. Food Eng. 311, 110709.

Barigou, M., 2004. Particle tracking in opaque mixing systems: an overview of the capabilities of PET and PEPT. Chem. Eng. Res. Des. 82 (9), 1258–1267.

Bauer, Werner, Nötzel, Dorit, Wenzel, Valentin, Nirschl, Hermann, 2015. Influence of dry mixing and distribution of conductive additives in cathodes for lithium ion batteries. J. Power Sources 288, 359–367.

Bockholt, Henrike, Indrikova, Maira, Netz, Andreas, Golks, Frederik, Kwade, Arno, 2016. The interaction of consecutive process steps in the manufacturing of lithium-ion battery electrodes with regard to structural and electrochemical properties. J. Power Sources 325, 140–151.

Buqa, H., Holzapfel, M., Krumeich, F., Veit, C., Novák, P., 2006. Study of styrene butadiene rubber and sodium methyl cellulose as binder for negative electrodes in lithium-ion batteries. J. Power Sources 161 (1), 617–622.

Grant, Patrick S., Greenwood, David, Pardikar, Kunal, Smith, Rachel, Entwistle, Thomas, Middlemiss, Laurence A., Murray, Glen, Cussen, Serena A., Lain, M.J., Capener, M.J., Copley, M., Reynolds, Carl D., Hare, Sam D., Simmons, Mark J.H., Kendrick, Emma, Zankowski, Stanislaw P., Wheeler, Samuel, Zhu, Pengcheng, Slater, Peter R., Zhang, Ye Shui, Morrison, Andrew R.T., Dawson, Will, Li, Juntao, Shearing, Paul R., Brett, Dan J.L., Matthews, Guillaume, Ge, Ruihuan, Drummond, Ross, Tredenick, Eloise C., Cheng, Chuan, Duncan, Stephen R., Boyce, Adam M., Faraji-Niri, Mona, Marco, James, Roman-Ramirez, Luis A., Harper, Charlotte, Blackmore, Paul, Shelley, Tim, Mohsseni, Ahmad, Cumming, Denis J., 2022. Roadmap on Li-ion battery manufacturing research. J. Phys.: Energy 4 (4), 042006 IOP Publishing.

Grießl, Desiree, Huber, Korbinian, Scherbauer, Raphael, Kwade, Arno, 2021. Dispersion kinetics of carbon black for the application in lithium-ion batteries. Adv. Powder Technol. 32 (7), 2280–2288.

Guida, Antonio, Nienow, Alvin W., Barigou, Mostafa, 2010. PEPT measurements of solid-liquid flow field and spatial phase distribution in concentrated monodisperse stirred suspensions. Chem. Eng. Sci. 65 (6), 1905–1914.

Hawley, W. Blake, Li, Jianlin, 2019. Electrode manufacturing for lithium-ion batteries–analysis of current and next generation processing. J. Energy Storage 25, 100862.

Cole, K., Brito-Parada, Pablo R., Hadler, Kathryn, Mesa, Diego, Neethling, Stephen J., Norori-McCormac, Alexander M., Cilliers, Jan J., 2022. Characterisation of solid hydrodynamics in a three-phase stirred tank reactor with positron emission particle tracking (PEPT). Chem. Eng. J. 433, 133819.

Kwade, Arno, Haselrieder, Wolfgang, Leithoff, Ruben, Modlinger, Armin, Dietrich, Franz, Droeder, Klaus, 2018. Current status and challenges for automotive battery production technologies. Nat. Energy 3 (4), 290–300 Number: 4 Publisher: Nature Publishing Group.

Lee, Jin-Hyon, Paik, Ungyu, Hackley, Vincent A., Choi, Young-Min, 2005. Effect of carboxymethyl cellulose on aqueous processing of natural graphite negative electrodes and their electrochemical performance for lithium batteries. J. Electrochem. Soc. 152 (9), A1763 IOP Publishing.

Rafiee, Marjan, Simmons, Mark J.H., Ingram, Andy, Hugh Stitt, E., 2013. Development of positron emission particle tracking for studying laminar mixing in Kenics static mixer. Chem. Eng. Res. Des. 91 (11), 2106–2113.

Martin, T.W., Seville, J.P.K., Parker, D.J., 2007. A general method for quantifying dispersion in multiscale systems using trajectory analysis. Chem. Eng. Sci. 62 (13), 3419–3428.

Nicuşan, A.L., Windows-Yule, C.R.K., 2020. Positron emission particle tracking using machine learning. Rev. Sci. Instrum. 91 (1), 013329.

Parker, D.J., Forster, R.N., Fowles, P., Takhar, P.S., 2002. Positron emission particle tracking using the new Birmingham positron camera. Nucl. Instrum. Methods Phys. Res., Sect. A 477 (1), 540–545.

Parker, David J., Fan, Xianfeng, 2008. A Positron emission particle tracking–Application and labelling techniques. Particuology 6 (1), 16–23.

Paul, Edward L., Atiemo-Obeng, Victor A., Kresta, Suzanne M., 2004. In: Paul, Edward L., Atiemo-Obeng, Victor A., Kresta, Suzanne M. (Eds.), Handbook of industrial mixing: science and practice. Wiley-Interscience 2004, Hoboken, N.J..

Pianko-Oprych, P., Nienow, A.W., Barigou, M., 2009. Positron emission particle tracking (PEPT) compared to particle image velocimetry (PIV) for studying the flow generated by a pitched-blade turbine in single phase and multi-phase systems. Chem. Eng. Sci. 64 (23), 4955–4968.

Reynolds, Carl D., Slater, Peter R., Hare, Sam D., Simmons, Mark J.H., Kendrick, Emma, 2021. A review of metrology in lithium-ion electrode coating processes. Mater. Des. 209, 109971.

Reynolds, Carl D., Hare, Sam D., Slater, Peter R., Simmons, Mark J.H., Kendrick, Emma, 2022. Rheology and structure of lithium-ion battery electrode slurries. Energy Technol. 10 (10), 2200545. https://doi.org/10.1002/ente.202200545

Simmons, M.J.H., Edwards, I., Hall, J.F., Fan, X., Parker, D.J., Stitt, E.H., 2009. Techniques for visualization of cavern boundaries in opaque industrial mixing systems. AIChE J. 55 (11), 2765–2772. https://doi.org/10.1002/aic.11889

Sung, SangHoon, Kim, Sunhyung, Park, JeongHoon, Park, JunDong, Ahn, KyungHyun, 2020. Role of PVDF in rheology and microstructure of NCM cathode slurries for lithium-ion battery. Materials 13 (20), 4544 Number: 20 Publisher: Multidisciplinary Digital Publishing Institute.

Wang, Ming, Dang, Dingying, Meyer, Andrew, Arsenault, Renata, Cheng, Yang-Tse, 2020. Effects of the mixing sequence on making lithium ion battery electrodes. J. Electrochem. Soc. 167 (10), 100518.

Werner, D., Davison, H., Robinson, E., Sykes, J.A., Seville, J.P.K., Wellings, A., Bhattacharya, S., Sanchez Monsalve, D.A., Kokalova Wheldon, T.Z., Windows-Yule, C.R.K., 2023. Effect of system composition on mixing in binary fluidised beds. Chem. Eng. Sci. 271, 118562.

Windows-Yule, C.R.K., Moore, A., Wellard, C., Werner, D., Parker, D.J., Seville, J.P.K., 2020a. Particle distributions in binary gas-fluidised beds: shape matters-But not much. Chem. Eng. Sci. 216, 115440.

Windows-Yule, C.R.K., Gibson, S., Werner, D., Parker, D.J., Kokalova, T.Z., Seville, J.P.K., 2020b. Effect of distributor design on particle distribution in a binary fluidised bed. Powder Technol. 367, 1–9.

Windows-Yule, Kit, Nicuşan, Leonard, Herald, Matthew T., Manger, Samuel, Parker, David, 2022. Positron Emission Particle Tracking: A comprehensive guide. IOP Publishing.

Windows-Yule, C.R.K., Seville, J.P.K., Ingram, A., Parker, D.J., 2020. Positron emission particle tracking of granular flows. Annu. Rev. Chem. Biomol. Eng. 11 (1), 367–396. https://doi.org/10.1146/annurev-chembioeng-011620-120633

Windows-Yule, C.R.K., Herald, M.T., Nicuşan, A.L., Wiggins, C.S., Pratx, G., Manger, S., Odo, A.E., Leadbeater, T., Pellico, J., de Rosales, R.T.M., Renaud, A., Govender, I., Carasik, L.B., Ruggles, A.E., Kokalova-Wheldon, T.Z., Seville, J.P.K., Parker, D.J., 2022. Recent advances in positron emission particle tracking: a comparative review. Rep. Prog. Phys. 85 (1), 016101 IOP Publishing.